https://doi.org/10.5194/hess-2019-192
Preprint. Discussion started: 4 June 2019

Hydrology and Earth System Sciences
Discussions

Required sampling-density of ground-based soil moisture and brightness temperature observations for calibration/validation of L-band satellite observations based on a virtual reality

Shaoning Lv[1*], Bernd Schalge[1], Pablo Saavedra Garfias[2], Clemens Simmer[1]

1. Institute for Geosciences and Meteorology at the University of Bonn, Auf dem Huegel 20, 53121 Bonn, Germany; 2. Geophysical Institute at the University of Bergen, Allégaten 70, 5020 Bergen, Norway.

Abstract: Microwave remote sensing is the most promising tool for monitoring global-scale near-surface soil moisture distributions. With the Soil Moisture and Ocean Salinity (SMOS) and Soil Moisture Active Passive (SMAP) missions in orbit, considerable efforts are made to evaluate their soil moisture products via ground observations, forward microwave transfer simulation, and retrievals. Due to the large footprint of the satellite radiometers of about 40 km in diameter and the spatial heterogeneity of soil moisture, minimum sampling densities for soil moisture are required to challenge the targeted precision. Here we use 400 m resolution simulations with the regional terrestrial system model TerrSysMP and its coupling with the Community Microwave Emission Modelling platform (CMEM) to quantify sampling distance required for soil moisture and brightness temperature validation. Our analysis suggests that an overall sampling resolution of better than 6 km is required to validate the targeted accuracy of 0.04 cm^3/cm^3 (70% confidence level) in SMOS and SMAP over typical midlatitude European regions. The minimum sampling resolution depends on the land-surface inhomogeneity and the meteorological situation, which influence the soil moisture patterns, and ranges from about 7 km to 17 km for a 70% confidence level for a typical year. At the minimum sampling resolution for a 70% confidence level also the accuracy of footprint-averaged brightness temperature estimates is equal or better than 15 K/10 K for H/V polarization. Estimates strongly deteriorate with sparser sampling densities, e.g., at 3/9 km with 3/5 sampling sites the confidence level of derived footprint estimates can reach about 0.5-0.6 for soil moisture which is much less than the standard 0.7 requirements for ground measurements. The representativeness of ground-based soil moisture and brightness temperature observations - and thus their required minimum sampling densities - are only weakly correlated in space and time. This study provides a basis for a better understanding of sometimes strong mismatches between derived satellite soil moisture products and ground-based measurements.

Key words: passive microwaves, soil moisture, brightness temperature, sampling density

https://doi.org/10.5194/hess-2019-192
Preprint. Discussion started: 4 June 2019

Hydrology and Earth System Sciences
Discussions

1. Introduction

Information on the global soil moisture distribution is required, e.g., for weather forecasting, climate, and agriculture applications. Due to the high spatial variability of soil moisture, its in-situ observation is practically impossible on continental scales. Passive microwave satellite remote sensing at L-band frequencies may achieve this goal because of the strong dependency of the soil dielectric constant on soil moisture at these wavelengths (Njoku and Kong, 1977;Ulaby et al., 1986). The first operational L-band soil moisture detection satellite SMOS (Soil Moisture and Ocean Salinity) was launched in 2008 (Kerr et al., 2010) and followed in 2015 by SMAP (Soil Moisture Active Passive), which additionally carries an active instrument to achieve higher spatial resolution (Entekhabi et al., 2010); the active component did fail, however, shortly after the full operation of the satellite. Both satellites are currently continuously observing passive microwave brightness temperatures from which soil moisture products are derived at tens of kilometers spatial resolution.

Before and after the launch of SMOS and SMAP several soil moisture monitoring networks for evaluation and retrieval algorithm development were set up, such as ESA's validation efforts at the Valencia Anchor Station (VAS) in eastern Spain and the upper Danube watershed located in southern Germany (Delwart et al., 2008;de Rosnay et al., 2006;Lemaitre et al., 2004), and the SMAP Cal/Val project (Brown et al., 2008;Delwart et al., 2008;Colliander et al., 2017a). According to the Level 1 baseline and minimum SMAP science requirements (SMAP Science Data Cal/Val Plan (O'Neill et al., 2015)) the spatial resolution of Level 2 (Passive Soil Moisture Product L2_SM_P) and Level 3 (daily composite L3_SM_P) soil moisture products is 36 km with an accuracy of 0.04 cm^3/cm^3. A wide range of measurement techniques and protocols exist for setting up and performing ground-based observations for evaluation. SMAP Cal/Val suggests that volumetric soil moisture should be observed in-situ at 5 cm and 100 cm depth while optimal sensing depths are still debated (Lv et al., 2016a;Lv et al., 2018). For core validation sites, a minimum of six - better 15 observations - over one SMAP grid cell or footprint is suggested (O'Neill et al., 2015;Famiglietti et al., 2008), but not substantiated yet by a thorough analysis (Jackson et al., 2012;Crow et al., 2012). Relevant studies typically use soil moisture networks with fixed resolutions over rather homogeneous land surfaces, which are not necessarily representative for all land surface types. For SMAP core calibration/validation sites a 36-km footprint should at least be sampled with eight stations leading to a 70% confidence for an estimated mean soil moisture uncertainty of 0.03 m^3/m^3 given a spatial variability of 0.07m^3/m^3. A 9-km footprint should at least be sampled with five stations leading to a 70% confidence for an estimated mean soil moisture uncertainty of 0.03 m^3/m^3, while a 3-km footprint should at least be sampled with three stations leading to a 70% confidence for an estimated 0.05 m^3/m^3 mean soil moisture uncertainty in both cases assuming a spatial soil moisture uncertainty of 0.05 m^3/m^3 within the respective footprints.

https://doi.org/10.5194/hess-2019-192
Preprint. Discussion started: 4 June 2019

Hydrology and Earth System Sciences
Discussions

Ochsner et al., 2013 point out that too few resources are currently devoted to in-situ soil moisture monitoring networks, and that despite their increasing number a standard for network density and sampling procedures is missing. Coopersmith et al., 2016 suggest temporary network extensions around permanent installations to quantify the representativeness of the latter. Qin et al., 2013 suggest the use of MODIS-derived apparent thermal inertia to interpolate between in-situ soil moisture measurements. So far, the required sampling density is discussed only concerning in-situ measurements, which heavily depend on sensor quality and network location (Vereecken et al., 2008;Brocca et al., 2010). No study is known to us, which investigates systematically the station density required for the evaluation of derived soil moisture or brightness temperatures taking the true land heterogeneity into account. In our study, we use a 400-m resolution virtual reality generated with a terrestrial modeling system coupled with an observation operator to estimate minimum station densities for the evaluation of L-band satellite observations and soil moisture retrieval products. This virtual reality allows us to arbitrarily vary the sampling resolution at steps of 400 m, which is impossible in field campaigns. Section 2 introduces our model-based virtual reality and the observation operator used to transfer terrestrial system states into virtual observations. In Section 3 we analyze the error growth with increasing sampling distances in time and space. Conclusions and discussion are provided in Section 4.

2. Methodology and data

2.1 Virtual reality

The modeling system used to create the virtual reality is the Terrestrial Systems Modeling Platform TerrSysMP (Shrestha et al., 2014;Gasper et al., 2014;Sulis et al., 2015) developed within the framework of the Transregional Collaborative Research Center 32 (TR32, Simmer, et al. 2015). TerrSysMP consists of the atmospheric model COSMO (Consortium For Small Scale Modelling, (Baldauf et al., 2011), the land surface model CLM (Community Land Model Version 3.5, (Oleson et al., 2008)), and the hydrological model ParFlow v693 (Ashby and Falgout, 1996;Kollet et al., 2010). The platform has especially been designed for high-performance computing environments (Gasper et al. 2014) and extensively evaluated against observations (Sulis et al. 2015, 2018; Shrestha et al. 2018b) and similar regional terrestrial system models (Sulis et al. 2017). The effect of spatial resolution on simulated soil moisture and resulting exchange fluxes between land and atmosphere has been studied with TerrSysMP by Shrestha et al. (2015, 2018a).

The simulated domain in this study is centered on the Neckar catchment in southwestern Germany (Figure 1). Notable features include the upper Rhine valley in the west, the Black Forest mountains in the southwest, and the foothills of the Alps in the southeast. The landscape has height variations of about 1100 m with lowest elevations found in the Rhine valley and highest in the Black Forest. The topographic data are obtained from the European Environment Agency EEA (http://www.eea.europa.eu/data-and-maps/data/eu-dem), which is also the source for the CORINE land use data (http://www.eea.europa.eu/data-and-maps/data/corine-land-cover-2006-raster-3) used to characterize vegetation in the model domain. Since CORINE uses many more land use classes than CLM, the CORINE classes are aggregated to five classes discriminated in the CLM: broadleaf forests which can be found

https://doi.org/10.5194/hess-2019-192
Preprint. Discussion started: 4 June 2019


Hydrology and Earth System Sciences
Discussions

mostly in hilly areas throughout the domain in smaller patches, needle leaf forests which dominate at higher elevation such as the Black Forest, grassland which is relatively rare and only appears in small patches, and crops which is the most dominant land use type throughout the domain and appears almost anywhere. All other classes such as urban areas are treated as bare soil in our study.

The Leaf Area Index (LAI) for the specific plant classes is taken from MODIS estimates corrected for known biases (Tian et al., 2004). We have not used the tiling approach in CLM; instead, we used the most dominant land use type for each grid-cell because the resolution is high enough to warrant this approach. The SAI is estimated from the LAI by a slightly modified formulation (no dead leaf for crops, constant base SAI of 10 % of maximum LAI) by (Lawrence and Chase, 2007) and (Zeng et al., 2002).

The soil map (Figure 1, upper row) is derived from a product of the German Federal Institute for Geosciences and Natural Resources BGR (http://www.bgr.bund.de/DE/Themen/Boden/Informationsgrundlagen/Bodenkundliche_Karten_Datenbanken/BUEK1000/buek1000_node.html). Soil values for regions near the edge of our domain in France and Switzerland were extrapolated. Variability was added to the relatively large polygons of constant soil parameters following Baroni et al. (2017) to represent better what would be found in reality at higher resolutions. The soil color was derived from the carbon content of the soil with carbon-rich soils being darker, except for the bare soil areas, which all use the same relatively light color class. There is deep soil geology included in ParFlow as well as alluvial channels below rivers to account for deeper subsurface flow, but these features will not directly impact the results shown here as they only appear below the soil layers.

CLM and ParFlow use the same horizontal computational grid with 400 m resolution. ParFlow has 50 vertical soil layers, the upper 10 of which coincide with the ten soil layers of CLM. The vertical resolution is variable with smaller steps near the land surface. The atmospheric model COSMO runs at a 1.1 km horizontal resolution which allows for convection permitting simulations. COSMO is forced at the lateral boundaries with a COSMO-DE analysis from the operational weather forecast runs from the German national weather service (Deutscher Wetterdienst, DWD) available at hourly time steps.

https://doi.org/10.5194/hess-2019-192
Preprint. Discussion started: 4 June 2019

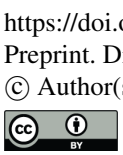

Hydrology and Earth System Sciences
Discussions

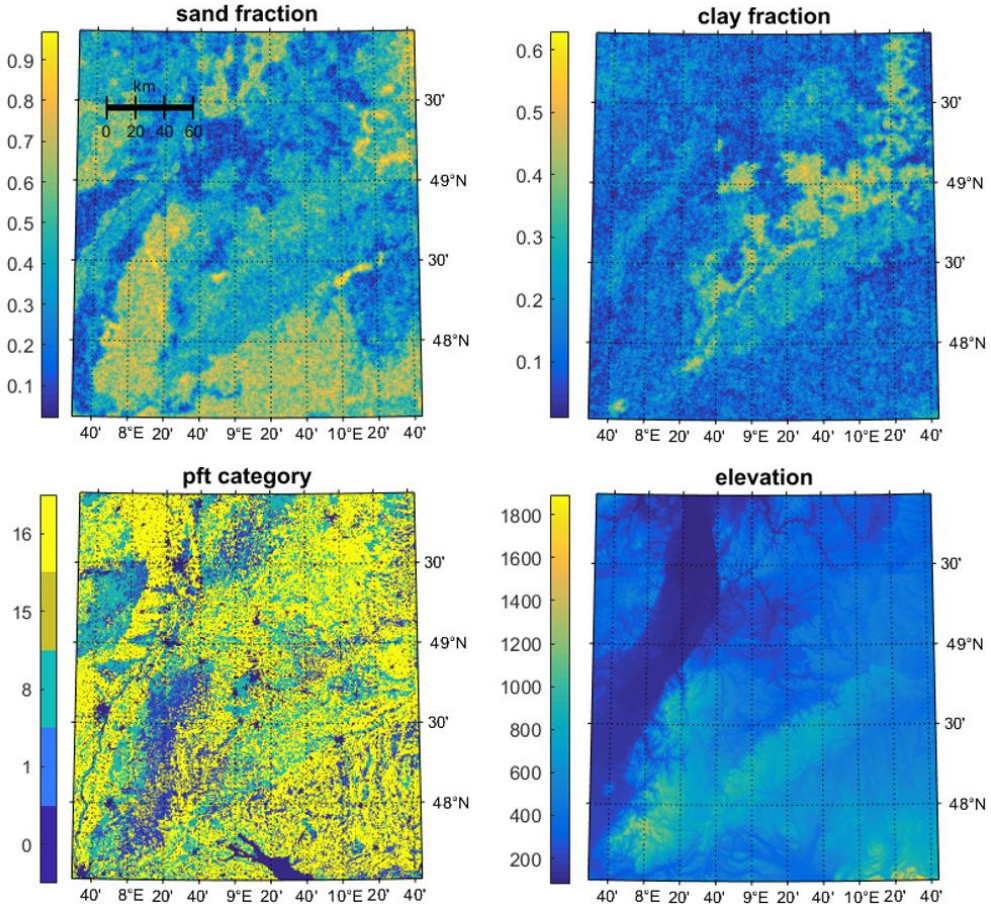

Figure 1: TerrSysMP simulation area at 400 m resolution with the Neckar catchment roughly in the center. Soil sand (left) and clay fractions (right) are displayed in the upper row sub-figures, while the Plant Functional Types (PTFs) used by CLM are shown in the lower left sub-figure (here we use a discrete scale representing the five classes including: 0 bare soil; 1 needle leaf evergreen temperate trees; 8 broadleaf deciduous temperate trees; 15 warm c4 grass; 16 crop) and topography (in m) in the lower right sub-figure.

131

132 **2.2 Generation of L-Band passive microwave observations**

133 The radiative transfer model CMEM (Rosnay et al., 2009) computes the land emissivity based on a
134 dielectric mixture model for soil moisture, soil sand and clay soil fractions, soil surface roughness,
135 vegetation optical thickness, single scattering albedo, and land surface orientation relative to the satellite
136 viewing perspective. Depending on the sand and clay fractions, brightness temperatures may vary by tens
137 of Kelvins given the same near-surface soil moisture. Vegetation optical thickness depends on LAI, which
138 varies in our virtual reality with time depending on PFT type. Also, soil temperature and snow depth (not

https://doi.org/10.5194/hess-2019-192
Preprint. Discussion started: 4 June 2019

Hydrology and Earth System Sciences
Discussions

shown) impact the simulated brightness temperatures. More details can be found, e.g., in the SMOS global surface emission model handbook (Rosnay et al., 2009).

From the 400 m resolution brightness temperatures, virtual satellite observations are generated taking the satellite antenna function into account. Figure 2 shows the centers of the about 320 footprints covering the model area for one potential satellite overpass and - on the same scale - the satellite antenna function for one footprint, which will change somewhat in shape with the elevation of the individual 400 m model grid areas, orbit, and satellite viewing angle.

Not each SMOS overflight will cover the whole area in reality. But in our study, we assume for simplicity, that all footprints indicated in Figure 2 are observed once a day at 6 a.m., which corresponds to the approximate descending or ascending overpass time of SMOS and SMAP, respectively. The satellite footprint is much larger than the nominal satellite spatial resolution of 40 km; thus areas much larger in diameter contribute to one satellite-observed brightness temperature (i.e., 50% of one satellite-observed brightness temperature originates from an area roughly ten times larger than the nominal satellite footprint).

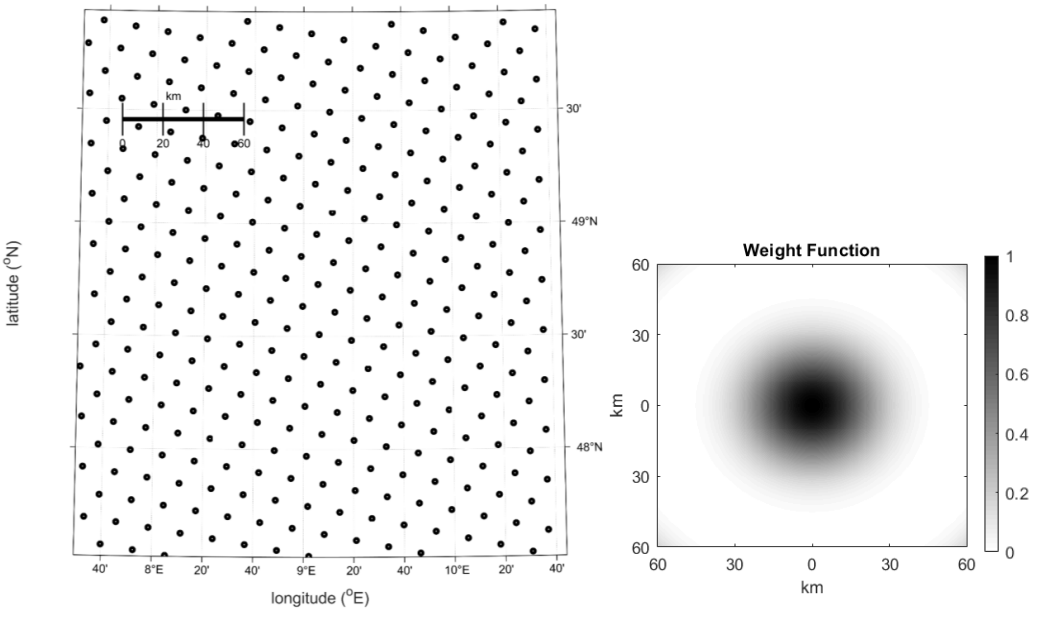

Figure 2: Dots in the left sub-figure indicate the centers of SMOS footprints for one hypothetical satellite overpass. The right sub-figure shows the antenna pattern in dB of one satellite footprint on the same scale as the map on the left.

The virtual reality employed in this study is a physically consistent state of the terrestrial system in space and time because it has been produced by a numerical model based on the conservations equations

https://doi.org/10.5194/hess-2019-192
Preprint. Discussion started: 4 June 2019

Hydrology and Earth System Sciences
Discussions

for mass, energy, and momentum. When applying the observation operator CMEM to this model state, we assume that the model state is correct and the simulated microwave transfer is error-free. Thus, our sampling study only quantifies the impact of the sampling density but does not include errors of the dynamic model (TerrSysMP) and/or the forward operator (CMEM). Based on the modeling results we analyze a range of ground-based network configurations with sampling points at least 400 m apart, and we assume that all quantities (state of the terrestrial system and brightness temperature) do not vary within 400 m. While this is an approximation, we believe that our results can be generalized, except that their outcome might be too optimistic.

With the model area covering one SMOS/SMAP footprint containing approximately 106x106 grid columns, that area could be sampled by one up to a maximum of 106x106 (virtual) sites. If the foot-print area is sampled with *n* sites, there are $C^{n}_{106x106}$ sampling combinations (SC, hereafter) possible, with

$$SC = C^{n}_{106x106} = \frac{106!}{n! \times (106-n)!} \quad (1)$$

which is an unordered collection of distinct elements of a prescribed size taken from a given set. For example, with an average distance between sampling sites of 10 km, about 6x6 sampling sites are possible within one footprint, which can be spatially distributed in $C^{6x6}_{106x106} \approx 1.69 \times 10^{104}$ ways. It is computationally not feasible to consider all those combinations. When we divide, however, first each footprint into equally-sized sub-areas, each containing exactly one sampling site (this assumes a certain homogeneity within the network), the number of potential sampling networks is drastically reduced. If we set, e.g., the average sampling distance of a 43-km wide footprint to *i* km, we divide the footprint into $\left(\frac{43}{i}\right)^2$ sub-areas each containing $106 \times 106 \Big/ \left(\frac{43}{i}\right)^2 \approx 6.08 \times i^2$ 400m-resolution model columns. When we further select within each sub-area of a satellite footprint the same model column (i.e., the one with row number *k* and column number *l*), a regular equidistant observation network within the SMOS/SMAP footprints is enforced similar to, e.g., the study by (Famiglietti et al., 2008). For each footprint (subscript f) at a particular time (subscript t) of a certain sampling distance (*i* km, subscript d), SC_{ftd} for soil moisture is

$$SC_{ftd} = \left(\frac{i}{0.4}\right)^2 \approx 106 \times 106 \Big/ \left(\frac{43}{i}\right)^2 \quad (2)$$

This results for a certain sampling distance (*i* km) for all 320 footprints and all 365 days of a year to

$$SC_{ft} = \left[106 \times 106 \Big/ \left(\frac{43}{i}\right)^2\right] \times 365 \times 320 \ . \quad (3)$$

For each day given two observations for all 320 footprints, we get

https://doi.org/10.5194/hess-2019-192
Preprint. Discussion started: 4 June 2019

$$SC_{td} = \sum_{i=0.8,1.2...}^{18} \left[106 \times 106 \Big/ \left(\frac{43}{i} \right)^2 \right] \times 320 \ , \quad (4)$$

and for each satellite footprint with two observations per day taken over one year

$$SC_{fd} = \sum_{i=0.8,1.2...}^{18} \left[106 \times 106 \Big/ \left(\frac{43}{i} \right)^2 \right] \times 365 \quad (5)$$

samples, from which we determine the one with the maximum sampling error. E.g., for 800 m sampling distance we determine the maximum from $\left(\frac{0.8}{0.4}\right)^2 \times 365 \times 320 \ = 467200$ samples, the number of which increases with the square of the sampling distance. This sampling is applied to both soil moisture and brightness temperature with and without considering the satellite weighting function (Figure 2b). The confidence level required by SMAP Cal/Val in core-sites is 70%. Thus, instead of the maximum error, we take the error at the 70 percentile, if not specified otherwise.

3. Results

We first discuss in detail the results for soil moisture sampling. Then we extend the same methodology to brightness temperature and compare both results. We also evaluate the potential sampling error for 3 km and 9 km satellite footprint sizes, because the SMAP products also include combined active-passive soil moisture retrievals at higher spatial resolutions (e.g., EASE-grid 9 km) and a product only based on the active sensor (EASE-grid 3 km).

3.1 Soil moisture

We compare the true (virtual) spatial arithmetic average of soil moisture at the SMOS/SMAP resolution with the arithmetic average of soil moisture computed from the sampling points taken at average distances ranging from 400 m (i.e., each TerrSysMP grid column, no sampling error) to 18 km (about half the radius of a SMAP or SMOS pixel. By Equation (3), (4), and (5), we analyze the sampling distance in the terms of Probability density function (Figure 3 and 6, based on SC_{ft}),along time dimension (Figure 4 and 7, based on SC_{td}) and along spatial dimension (Figure 5 and 8, based on SC_{fd}). When we later compare brightness temperatures we use averages weighted by the antenna function; using that strategy also for soil moisture leads to differences below 0.01 cm^3/cm^3; thus the averaging procedure does not impact our conclusions for soil moisture.

For each average sampling distance, we compute for each footprint the maximum sampling error obtained from the twice-daily observations over one year of all network configurations. The distribution of the corresponding 320 values is displayed in Figure 3 (top). Thus each value entering the distribution at a given average sampling distance (individual box plot in Figure 3) stems from that sampling network for one of the 320 SMOS/SMAP footprints, which leads to the largest sampling error taking all twice-daily

https://doi.org/10.5194/hess-2019-192
Preprint. Discussion started: 4 June 2019


Hydrology and Earth System Sciences
Discussions

observations over a year into account (Equation (3)). With a sampling distance of 400m, we exactly reproduce the true (virtual) arithmetic soil moisture average, i.e., the maximum error is zero. Maximum errors increase with sampling distance as demonstrated by the widening of the maximum error distribution. The median of the maximum sampling error increases about linearly with about 0.022 cm^3/cm^3 per kilometer sampling distance. The spread of the maximum error increases from less than 0.01 cm^3/cm^3 at 0.8 km to 0.4 cm^3/cm^3 at 18 km with quite some variability between the sampling steps. To guarantee an absolute error below 0.04 cm^3/cm^3 (the assumed accuracy of SMOS/SMAP retrievals) , which with 100% confidence everywhere in the region at any time of the year, the maximum average sampling distance should not exceed 2.8 km. At an average sampling distance of 4.8 km, for 50% of the SMOS/SMAP pixels sampling networks exist, which would lead to the occurrence of sampling errors above 0.04 cm^3/cm^3 at least once per year. At an average sampling distance of 4.4 km (less than 18 sites within a 43 km x 43 km pixel), the same would hold for more than 75% of the SMOS pixels. We note here that the size of the average footprints of the SMAP passive soil moisture product is 36 km x 36 km per pixel which is somewhat less than for SMOS.

For SMAP CAL/VAL core validation sites the target accuracy should be reached with a confidence level of only 70%. Figure 3 (bottom) displays the distribution of the 70 percentile of the error at each satellite pixel instead of the maximum error (100 percentile) shown in Figure 3 (top). Thus, to guarantee an error below 0.04 cm^3/cm^3 for all network configurations for only up to 70% of all SMOS/SMAP pixels and all days of the year, a minimum sampling distance of 6 km is required. At an average sampling distance of 12 km, only 50% of the pixels fulfill this requirement. Overall, about one-quarter of the nominal stations are needed, when the requirement to stay within the 0.04 cm^3/cm^3 error margin is relaxed from 100% confidence level to 70%.

https://doi.org/10.5194/hess-2019-192
Preprint. Discussion started: 4 June 2019

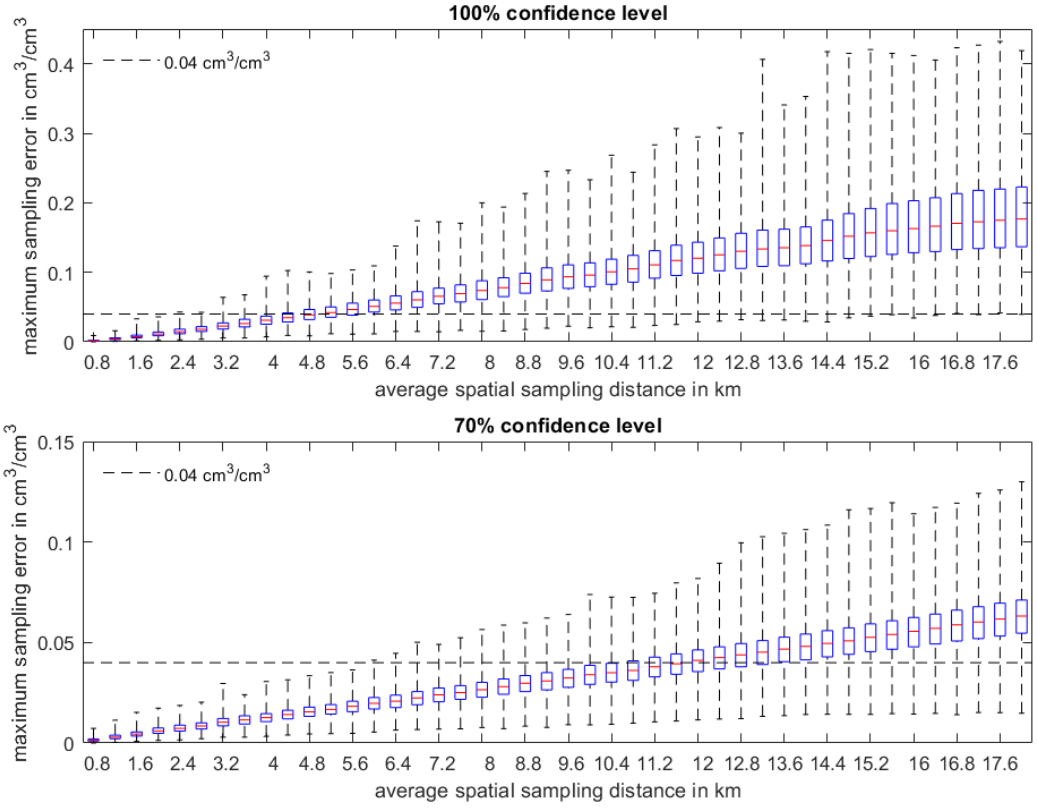

Figure 3: Box-whisker-plots (median in red, 25- and 75-percentiles as bounds of the box, whiskers encompass all values) of the maximum sampling errors for the 320 satellite footprints of the arithmetic mean soil moisture estimated for all network configurations observing twice-a-day over one year at given average sampling distances (abscissa). The top subfigure shows the absolute maximum error, while the bottom subfigure displays the results for the 70th percentile of the error at each satellite footprint. The horizontal dashed line is the 0.04 cm^3/cm^3 retrieval error anticipated for SMOS and SMAP.

From the simulations, we can also quantify the required maximum sampling distance for each daily observation of the whole area, and for each of the 320 SMOS/SMAP footprints over time by the samples defined in Equation (4). According to Figure 4, for 80 percent of the SMOS/SMAP pixels, the maximum sampling distance is between 8.4 km and 16 km, which is 7 - 26 stations for SMOS (43 km) and 5 - 18 stations for SMAP passive (36 km) to reach the 70% confidence level. A seasonal variation is not obvious, but rainfall events affect the distributions by increasing the maximum sampling distances because the surface soil moisture becomes more homogeneously distributed in space. The opposite occurs during drought events, because of evaporation, draining, and runoff tends to create spatially inhomogeneous soil moisture distributions.

https://doi.org/10.5194/hess-2019-192
Preprint. Discussion started: 4 June 2019

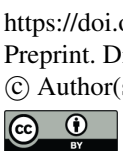

Hydrology and Earth System Sciences
Discussions

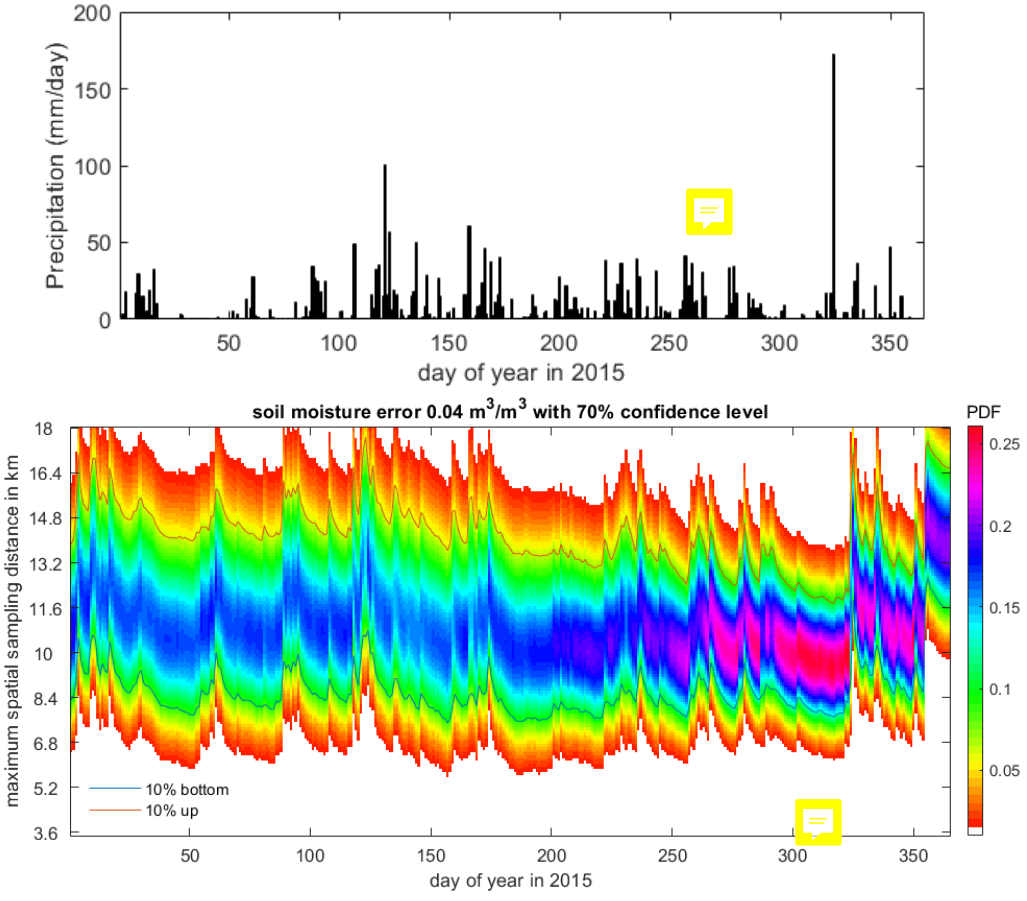

Figure 4: Time series of the distribution of the maximum soil moisture sampling distance for each SMOS/SMAP pixel required to assure a sampling error below 0.04 cm^3/cm^3 (70% confidence) for the year 2015. The grey intensity is proportional to the probability of occurrence. Also the median and the 5 and 95-percentiles are indicated as lines.

246

247 The spatial distribution of the annual average maximum sampling distance required to guarantee a
248 sampling error below 0.04 cm^3/cm^3 (70% confidence) and its RMS for the year 2015 (Figure 5) indicates,
249 that the southeastern region requires on average sampling distances of up to 16 km; thus only nine sites
250 are required within a SMOS/SMAP pixel to estimate the footprint-averaged soil moisture with a sampling
251 error below 0.04 cm^3/cm^3. However, the annual variation is particularly small (blue). For the rest of the
252 region, maximum sampling distances range from 7 km to 10 km; thus, many more than nine sites are
253 required within one footprint. The annual variation of the maximum sampling distances for those
254 footprints is larger than in the southeast. The mean sampling distances and their day-to-day variations
255 are only weakly correlated (correlation coefficient 0.40), but show larger-scale common patterns.

https://doi.org/10.5194/hess-2019-192
Preprint. Discussion started: 4 June 2019

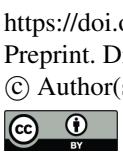

Hydrology and Earth System Sciences
Discussions

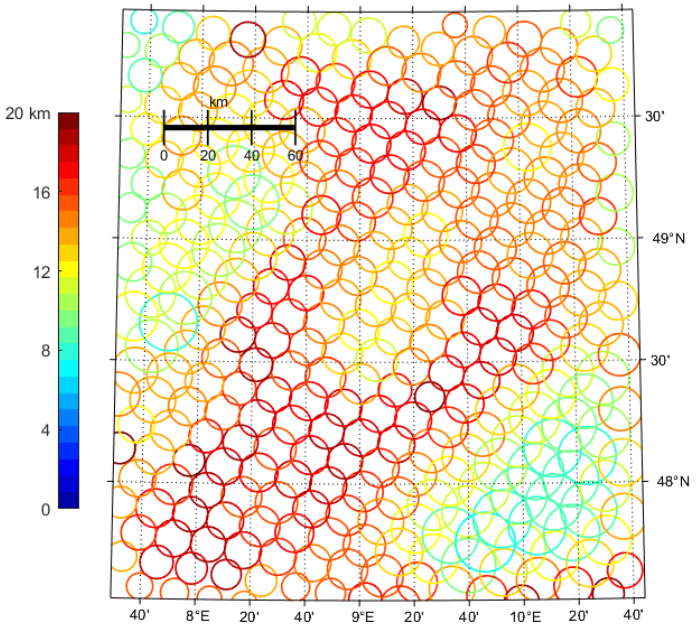

Figure 5: Spatial distribution of the mean soil moisture sampling distance in the model area required for keeping the maximum sampling error below 0.04 m^3/m^3 over the whole year. The circle diameter indicates the maximum sampling distance in the scale shown in the map, while its color (see color bar) gives the RMS of the maximum sampling distance over time for the year 2015.

3.2 brightness temperature

We now determine the maximum sampling distances of ground-based microwave radiometers observing the land surface required to estimate SMOS/SMAP footprint brightness temperatures. To this goal, we transform the target accuracy of SMOS/SMAP soil moisture retrievals of 0.04 cm^3/cm^3 to the accuracy of the corresponding brightness temperature, which is 10 K for H polarization and 5 K for V polarization according to CMEM forward simulations. We note that this brightness temperature accuracy is not the instrument observing error of the (virtual) microwave radiometer, but the sensitivity of the microwave forward transfer model to soil moisture. We are aware, that the radiometric accuracies of ground-based and satellite-borne sensors are much better, and that the accuracy of the soil moisture-brightness temperature relation is mainly responsible for the retrieval accuracy; thus we use the 10K/5K uncertainty only as a proxy for the overall error.

According to Figure 6 already at a sampling distance of 800 m, the sampling error might exceed the 10K/5K limit at certain regions and times. If we want to keep the limit with a probability of 90% (the upper boundary of boxes in Figure 6 H/V 100% confidence panels), a maximum sampling distance below 4.4 km/4 km will confine the sampling error to below 10 K/5 K for H/V polarization brightness temperatures.

https://doi.org/10.5194/hess-2019-192
Preprint. Discussion started: 4 June 2019

Hydrology and Earth System Sciences
Discussions

For an average sampling distance of 5.2 km, the error may go beyond the nominal 10 K/5 K for both polarizations already with a probability of 50%, and already for 9.2 km average sampling distance, the maximum sampling error is always above the nominal values for some region and a day in the year. Even if we relax the nominal error to only 70% of all pixels and days, the requirement cannot be met already at 800 m average sampling distance, while the average sampling distance required to fulfill the nominal accuracy for only 50% of all networks moves from 5.2 to 10 km.

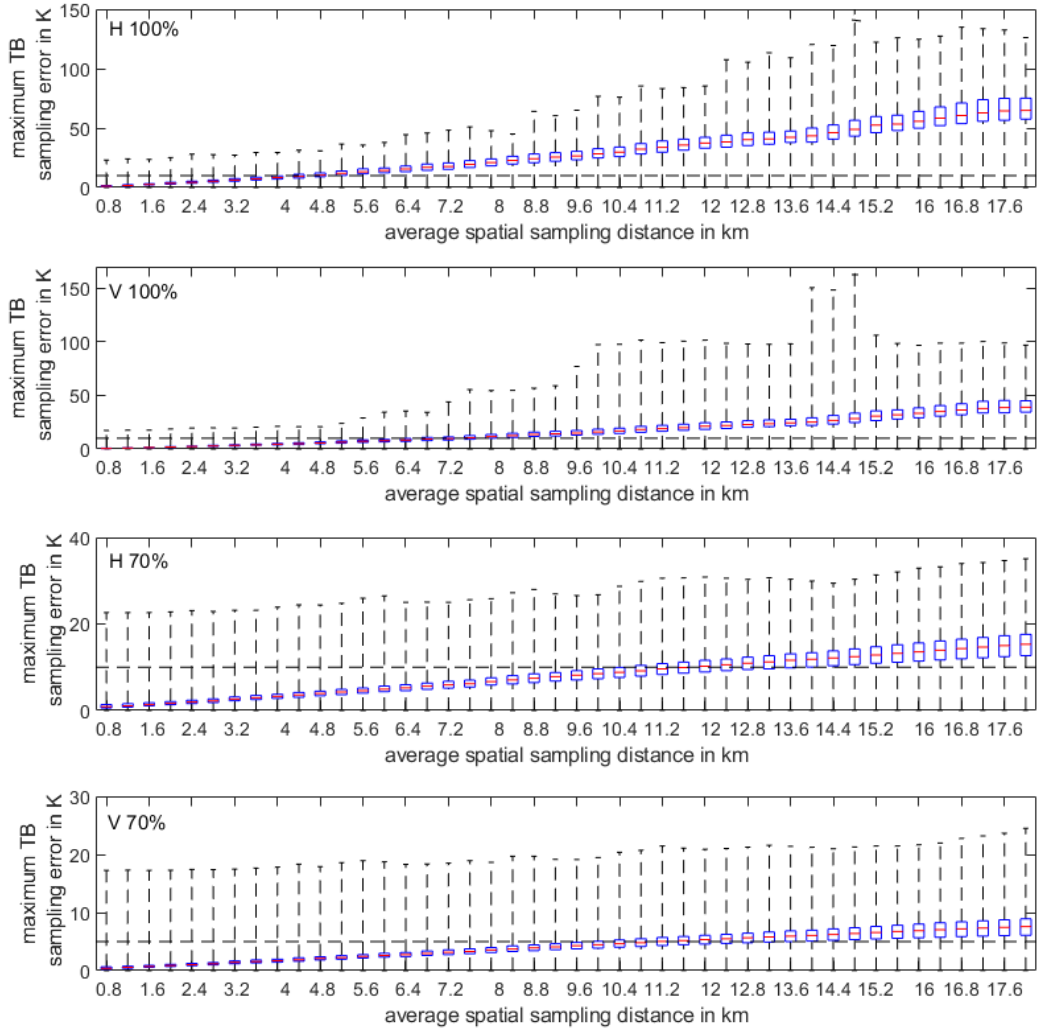

Figure 6: Same as Figure 3 but for the sampling error of the brightness temperature. The respective brightness temperature errors equivalent to a soil moisture accuracy of 0.04 cm^3/cm^3 of 10 K for H polarization and 5 K for V polarization are indicated as dashed horizontal lines.

https://doi.org/10.5194/hess-2019-192
Preprint. Discussion started: 4 June 2019

Hydrology and Earth System Sciences
Discussions

279 The time series of the distribution of the maximum sampling distances for brightness temperature
280 (Figure 7) is quite similar to the one for the maximum sampling distances for soil moisture. Values range
281 from 6.8 km to 16.4 km for most cases. The spread of the sampling error has, however, a distinct seasonal
282 variation; e.g., the maximum sampling distance for 90% of the sampling configurations is 11.6 km from
283 DOY 100 to 275 and 8.8 km for the rest of the year.

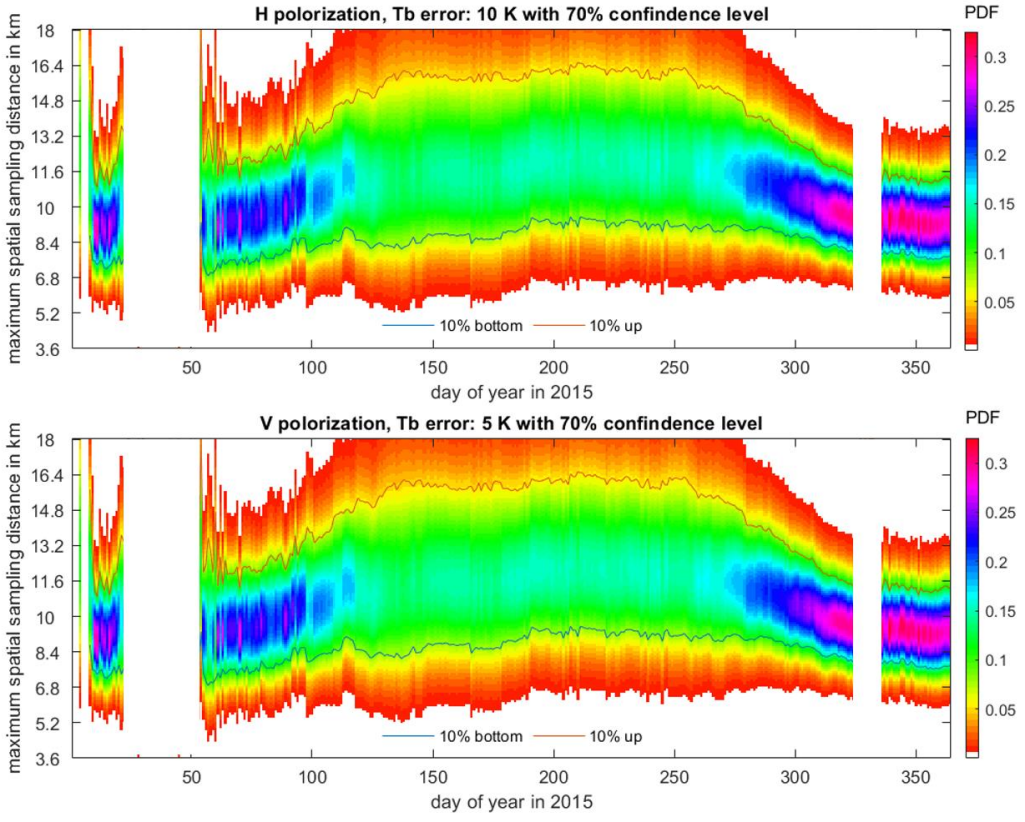

Figure 7: Time series of the distribution of maximum sampling distances (70% confidence in 10K/5K for H/V polorization) for brightness temperature at every sites in 2015. The degree of grayness indicates the probability of occurrence.

284

285 The spatial distribution of the annual average maximum sampling distance required to guarantee a
286 sampling error below 10K/5K for H/V polarized brightness temperatures and its RMS for the year 2015
287 (Figure 8) are similar for H and V polarizations but show different and much stronger patterns compared
288 to the results for soil moisture (Figure 5). Similarly, the southeast corner of the model region has larger
289 maximum sampling distances, but there are now also other distinct regions with larger minimum sampling
290 distances. Additional input parameters required and internal parameters in CMEM now impact the
291 representativeness of different sites - especially LAI. LAI dominates the variation of the representativeness

https://doi.org/10.5194/hess-2019-192
Preprint. Discussion started: 4 June 2019

Hydrology and Earth System Sciences
Discussions

of ground-based observations and also its temporal variation, as can be inferred from the correlation between large maximum sampling distances with its variability over the year (correlation coefficient is 0.84/0.83 for H/V polarization), which is not observed for soil moisture. LAI is the only input in CMEM which can lead to such a temporal variation because other inputs and internal parameters such as air temperature, soil moisture, soil properties, etc. are either fixed or do not impact on brightness temperature significantly.

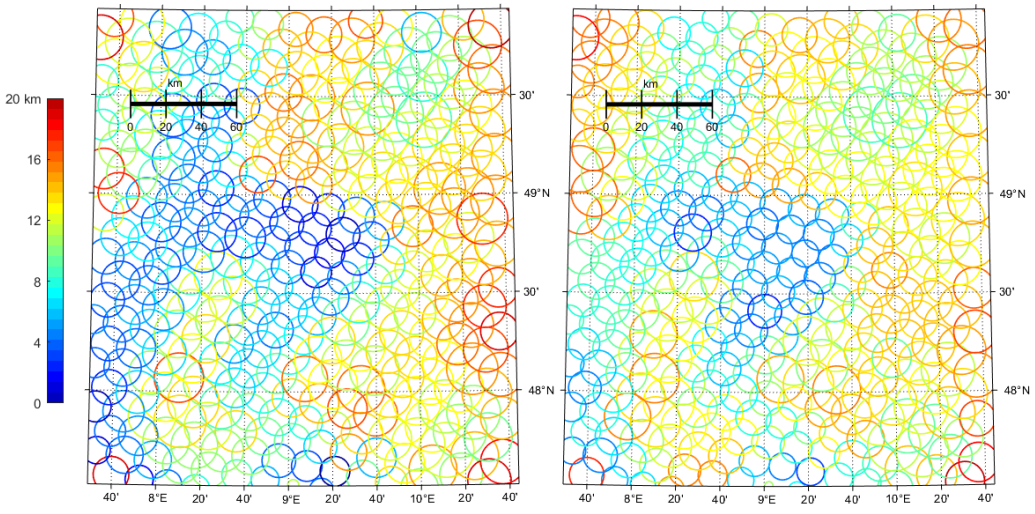

Figure 8: Spatial distribution of the surface-based brightness temperature network resolution required in the model region. The circle diameter indicates the maximum sampling distance which keeps the error below 10 K for H polarization and 5 K for V polarization in the scale shown in the map, while its color (see color bar) gives the RMS of the maximum sampling distance over time for the year 2015.

3.3 Maximum sampling distance differences between soil moisture and brightness temperature

The differences in the variability of the maximum sampling distance for soil moisture and brightness temperature can be explained by using the microwave transfer model CMEM. The relationship between soil moisture and brightness temperature is complex and non-unique (Figure 9a, b). E.g., a soil moisture value of 0.4 cm^3/cm^3 can relate to a wide range of brightness temperature from 180 K to 250 K for H polarization and 225 K to 265 K for V polarization due to the variation of vegetation cover, soil properties, and terrain.

https://doi.org/10.5194/hess-2019-192
Preprint. Discussion started: 4 June 2019

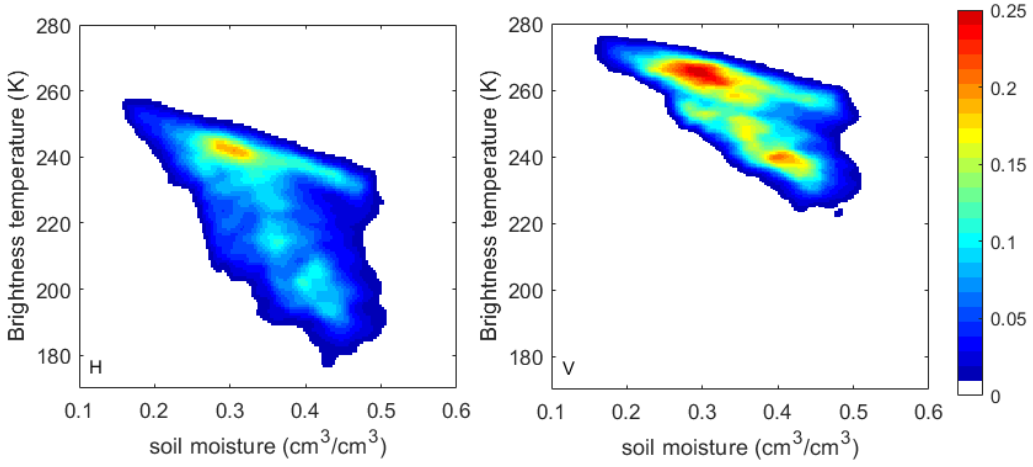

Figure 9: Scatter plots of joint PDF between brightness temperature at H and V polarization against soil moisture computed from the 400 m resolution virtual reality for one year. Both temporal and spatial variation are accounted.

307

308 The spatial resolution for the SMAP active product is 3 km and for the passive-active merged soil
309 moisture product 9 km. SMAP CAL/VAL requires for core stations 3 stations for the evaluation of the prior
310 and 5 stations for the latter product. We computed the average station distance for both products
311 required to keep the sampling error below the nominal 0.04 cm^3/cm^3 by using the same methodology
312 used above. Due to limited computation capacity, not all higher-resolution footprints are used, but only
313 those in the center of the 43-km SMOS footprints. According to the results displayed in Figure 10, the
314 confidence level for most of the 3/9-km footprints sampled by 3/5 stations is below 50%-60% and thus
315 lower than the required 70%. The temporal variation of the confidence level is larger for the 3 km than
316 for the 9 km footprints.

https://doi.org/10.5194/hess-2019-192
Preprint. Discussion started: 4 June 2019

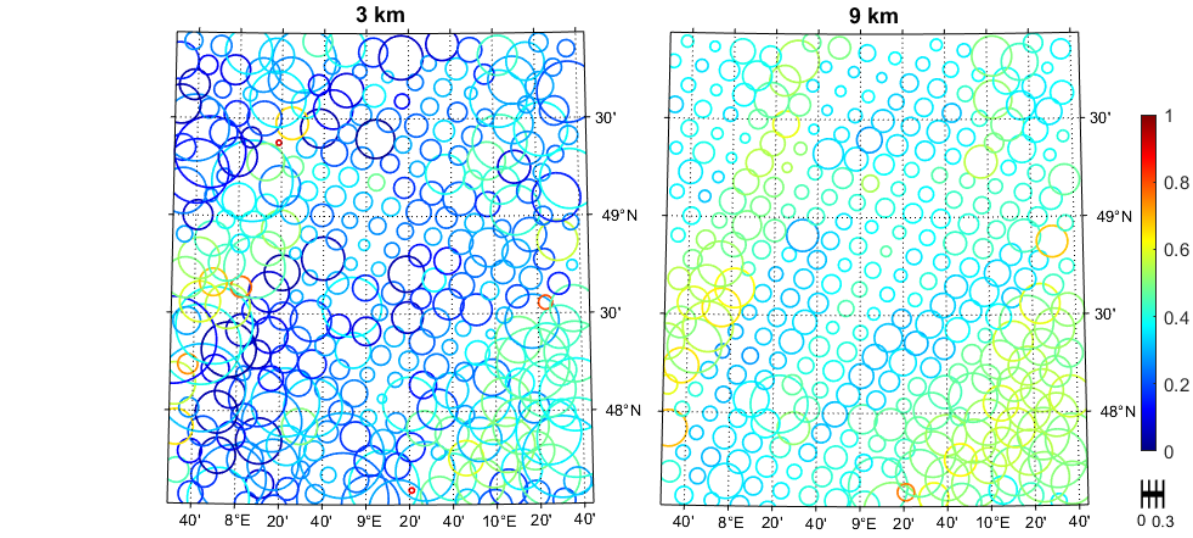

Figure 10: The spatial distribution of the soil moisture sampling confidence to achieve the 0.04 cm^3/cm^3 accuracy requirement by sampling 3/9-km footprints with 3/5 sites. The colors show the minimum confidence level throughout the year 2015 for every footprint. The size of circles indicate the standard deviation of the confidence level over the time.

3.4 The impact of land surface inhomogeneity

Areas with vegetation water content > 5 kg/m^2 (mostly forests) are flagged in SMAP retrievals. The networks used in the studies by (Colliander et al., 2017b; Famiglietti et al., 2008) were selected based on homogeneity; thus forested patches, open water, permanent ice and snow, urban areas, wetlands are excluded. Soil moisture maps from SMAP/SMOS are, however, global. Thus estimates are provided everywhere; thus signals from open water surfaces on sub-grid scales may influence the products. We used our simulated observations to study the impact of sub-pixel contributions of forested areas on the sampling errors.

In total 16 of the 320 footprints in the model area have forest fractions below 15% and negligible surface water contributions; such footprints are usually considered as an ideal footprint for soil moisture Cal/Val. We compare their sampling statistics with the statistics for all footprints in Figure 11, which shows that in terms of both soil moisture and brightness temperature, the maximum sampling errors for the selected sites are considerably lower compared all sites for all sampling distances. Thus, excluding sites with forest fractions above 15% is beneficial for both soil moisture and brightness temperature evaluations.

https://doi.org/10.5194/hess-2019-192
Preprint. Discussion started: 4 June 2019

Hydrology and Earth System Sciences
Discussions

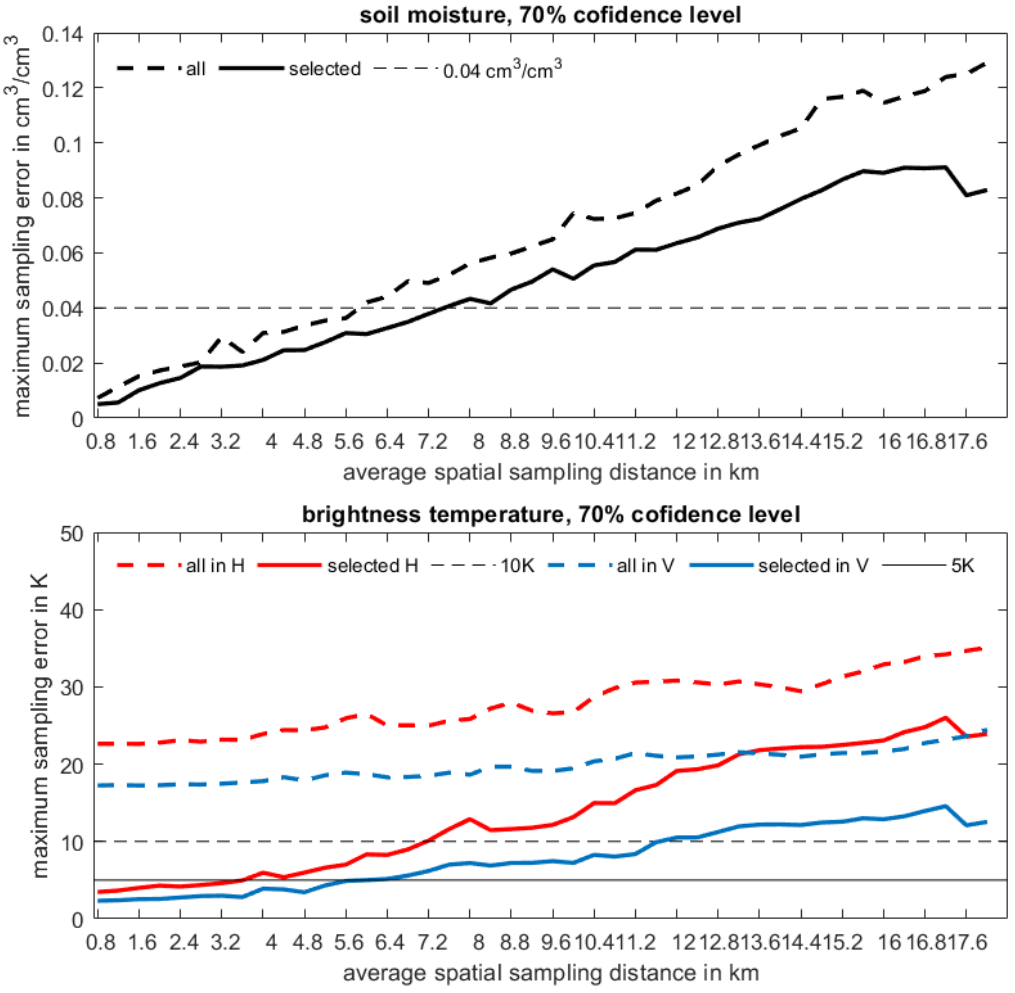

Figure 11: The maximum sampling errors of the arithmetic mean soil moisture/brightness temperature estimated from all sites and from sites with < 15% forest cover at given average sampling distances.

4. Conclusion and discussion

We used a virtual reality generated with the fully coupled subsurface-vegetation-atmosphere model platform TerrSysMP over southwestern Germany with a spatial resolution of 400 m to quantify the sampling error of mean soil moisture and brightness temperatures estimated from in-situ ground-based observation networks covering the 43 km x 43 km SMOS/SMAP-like footprints over a wide range of potential average sampling distances. By using a simulated virtual reality at such a high resolution, we have a physically consistent three-dimensional evolution of the terrestrial system at our disposition, from which we can take virtual soil moisture observations at any resolution at and above 400 m, and we can

https://doi.org/10.5194/hess-2019-192
Preprint. Discussion started: 4 June 2019


Hydrology and Earth System Sciences
Discussions

simulate SMOS/SMAP-like observations taking into account the antenna function and the microwave radiative transfer model CMEM.

A comparison between the representativeness of ground-based soil moisture and brightness temperature observation networks reveals the complexity behind the sampling density issue. We adopted as an upper threshold for the sampling error of the estimated soil moisture and brightness temperature for SMOS/SMAP pixels the target SMOS/SMAP soil moisture retrieval accuracy of 0.04 cm^3/cm^3. We quantified the maximum sampling distance of ground-based observations required to keep the sampling error below that accuracy for all and for 70% of the SMOS/SMAP pixels over the modeling region and over one year for all network configurations possible for the specified average sampling distances.

The calibration and validation of L-band passive remote sensing of soil moisture is difficult due to its large variability (Lv et al., 2019; Lv et al., 2016b). Even with a perfect microwave transfer model and perfect sensors, we can hardly find a appropriate in-situ observation to compare with. While soil moisture also varies in the vertical, sensors are usually mounted at a fixed depth; thus comparisons with satellite observations require the knowledge of the microwave penetration depth, which is however unknown in general. Lv et al. (2018) developed a model based on the soil effective temperature, which sheds light on this fundamental problem. The SMAP team suggests 15 sites for a 36 km by 36 km footprint, and this study agrees with this configuration for typical midlatitude European regions. However, 5 sites for 9 km by 9 km and 3 sites for 3 km by 3 km will miss the 70 % confidence level requirements over this area.

It is difficult to set up an observation network, which represents the whole satellite footprint precisely. We find a maximum soil moisture sampling distance of roughly 3 km if we want to be 100% sure that the sampling error is below the nominal value of 0.04 cm^3/cm^3. If we allow for a failure probability of 30 % a maximum sampling distance of 10 km is sufficient. For brightness temperatures, the sampling requirement is much stricter, because already at 800 m sampling distance, it cannot be guaranteed, that the sampling error remains below the equivalent threshold of 10K/5K for H and V-polarization, respectively, even for a 30% probability of failure.

While the required maximum sampling distances do not change much over the year for soil moisture - except after large-scale precipitation events which allow for larger sampling distances - its equivalent for brightness temperature has a strong seasonal variation because of the blurring effect of vegetation during the growing season when brightness temperatures become more homogeneous. The spatial distribution of the maximum sampling distances and their local variances behave quite differently between soil moisture and brightness temperature. The spatial patterns are different, and while the maximum sampling distance and its variance are strongly related for brightness temperature, they are barely related for soil moisture; this different behavior is caused by the complexity of other factors influencing microwave radiative transfer. Our study strongly suggests that the sampling density of current SMOS/SMAP ground-based Cal/Val networks should be reviewed carefully and the resulting potential

sampling error of estimated pixel-mean soil moisture and brightness temperatures considered in such studies. We expect this study will help to better understand the errors of satellite-derived soil moisture.

Acknowledgments

This research was funded by the Deutsche Forschungsgemeinschaft (DFG) via FOR2131: "Data Assimilation for Improved Characterization of Fluxes across Compartmental Interfaces", subproject P2. Compute time has been provided by the Gauss Centre for Supercomputing (http://www.gauss-centre.eu/gauss-centre/EN/Home/home_node.html) operated by the Juelich Supercomputing Centre (http://www.fz-juelich.de/ias/jsc/EN/Home/home_node.html). We thank the members of HPSC-TerrSys (http://www.hpsc-terrsys.de/hpsc-terrsys/EN/Home/home_node.html) and Klaus Goergen in particular for invaluable technical support with the JUQUEEN supercomputer. Furthermore, we thank Prabhakar Shresta and Mauro Sulis from the Transregional Collaborative Research Center 32 (TR32) for their preliminary work and introduction to the TerrSysMP modeling platform.

References

Ashby, S. F., and Falgout, R. D.: A parallel multigrid preconditioned conjugate gradient algorithm for groundwater flow simulations, Nucl Sci Eng, 124, 145-159, 1996.

Baldauf, M., Seifert, A., Förstner, J., Majewski, D., Raschendorfer, M., and Reinhardt, T.: Operational convective-scale numerical weather prediction with the COSMO model: Description and sensitivities, Monthly Weather Review, 139, 3887-3905, 2011.

Brocca, L., Melone, F., Moramarco, T., and Morbidelli, R.: Spatial-temporal variability of soil moisture and its estimation across scales, Water Resources Research, 46, 10.1029/2009wr008016, 2010.

Brown, M. A., Torres, F., Corbella, I., and Colliander, A.: SMOS calibration, Ieee Transactions on Geoscience and Remote Sensing, 46, 646-658, Doi 10.1109/Tgrs.2007.914810, 2008.

Colliander, A., Cosh, M. H., Misra, S., Jackson, T. J., Crow, W. T., Chan, S., Bindlish, R., Chae, C., Collins, C. H., and Yueh, S. H.: Validation and scaling of soil moisture in a semi-arid environment: SMAP validation experiment 2015 (SMAPVEX15), Remote Sensing of Environment, 196, 101-112, 10.1016/j.rse.2017.04.022, 2017a.

Colliander, A., Jackson, T. J., Bindlish, R., Chan, S., Das, N., Kim, S. B., Cosh, M. H., Dunbar, R. S., Dang, L., Pashaian, L., Asanuma, J., Aida, K., Berg, A., Rowlandson, T., Bosch, D., Caldwell, T., Caylor, K., Goodrich, D., al Jassar, H., Lopez-Baeza, E., Martínez-Fernández, J., González-Zamora, A., Livingston, S., McNairn, H., Pacheco, A., Moghaddam, M., Montzka, C., Notarnicola, C., Niedrist, G., Pellarin, T., Prueger, J., Pulliainen, J., Rautiainen, K., Ramos, J., Seyfried, M., Starks, P., Su, Z., Zeng, Y., van der Velde, R., Thibeault, M., Dorigo, W., Vreugdenhil, M., Walker, J. P., Wu, X., Monerris, A., O'Neill, P. E., Entekhabi, D., Njoku, E. G., and Yueh, S.: Validation of SMAP surface soil moisture products with core validation sites, Remote Sensing of Environment, 191, 215-231, https://doi.org/10.1016/j.rse.2017.01.021, 2017b.

Coopersmith, E. J., Cosh, M. H., Bell, J. E., Kelly, V., Hall, M., Palecki, M. A., and Temimi, M.: Deploying temporary networks for upscaling of sparse network stations, Int. J. Appl. Earth Obs. Geoinf., 52, 433-444, 10.1016/j.jag.2016.07.013, 2016.

Cosh, M. H., Jackson, T. J., Bindlish, R., and Prueger, J. H.: Watershed scale temporal and spatial stability of soil moisture and its role in validating satellite estimates, Remote Sensing of Environment, 92, 427-435, 10.1016/j.rse.2004.02.016, 2004.

https://doi.org/10.5194/hess-2019-192
Preprint. Discussion started: 4 June 2019

Crow, W. T., Berg, A. A., Cosh, M. H., Loew, A., Mohanty, B. P., Panciera, R., de Rosnay, P., Ryu, D., and Walker, J. P.: Upscaling sparse ground-based soil moisture observations for the validation of coarse-resolution satellite soil moisture products, Reviews of Geophysics, 50, 20, 10.1029/2011rg000372, 2012.

de Rosnay, P., Calvet, J. C., Kerr, Y., Wigneron, J. P., Lemaitre, F., Escorihuela, M. J., Sabater, J. M., Saleh, K., Barrie, J. L., Bouhours, G., Coret, L., Cherel, G., Dedieu, G., Durbe, R., Fntz, N. E. D., Froissard, F., Hoedjes, J., Kruszewski, A., Lavenu, F., Suquia, D., and Waldteufel, P.: SMOSREX: A long term field campaign experiment for soil moisture and land surface processes remote sensing, Remote Sensing of Environment, 102, 377-389, 10.1016/j.rse.2006.02.021, 2006.

Delwart, S., Bouzinac, C., Wursteisen, P., Berger, M., Drinkwater, M., Martin-Neira, M., and Kerr, Y. H.: SMOS validation and the COSMOS campaigns, Ieee Transactions on Geoscience and Remote Sensing, 46, 695-704, 2008.

Entekhabi, D., Njoku, E. G., O'Neill, P. E., Kellogg, K. H., Crow, W. T., Edelstein, W. N., Entin, J. K., Goodman, S. D., Jackson, T. J., Johnson, J., Kimball, J., Piepmeier, J. R., Koster, R. D., Martin, N., McDonald, K. C., Moghaddam, M., Moran, S., Reichle, R., Shi, J. C., Spencer, M. W., Thurman, S. W., Tsang, L., and Van Zyl, J.: The Soil Moisture Active Passive (SMAP) Mission, P Ieee, 98, 704-716, 10.1109/jproc.2010.2043918, 2010.

Famiglietti, J. S., Ryu, D. R., Berg, A. A., Rodell, M., and Jackson, T. J.: Field observations of soil moisture variability across scales, Water Resources Research, 44, 10.1029/2006wr005804, 2008.

Gasper, F., Goergen, K., Shrestha, P., Sulis, M., Rihani, J., Geimer, M., and Kollet, S.: Implementation and scaling of the fully coupled Terrestrial Systems Modeling Platform (TerrSysMP v1. 0) in a massively parallel supercomputing environment–a case study on JUQUEEN (IBM Blue Gene/Q), Geosci. Model Dev., 7, 2531-2543, 2014.

Jackson, T., Colliander, A., Kimball, J., Reichle, R., Crow, W., Entekhabi, D., and Neill, P.: Science data calibration and validation plan, Jet Propuls. Lab, 2012.

Kerr, Y. H., Waldteufel, P., Wigneron, J. P., Delwart, S., Cabot, F., Boutin, J., Escorihuela, M. J., Font, J., Reul, N., Gruhier, C., Juglea, S. E., Drinkwater, M. R., Hahne, A., Martin-Neira, M., and Mecklenburg, S.: The SMOS Mission: New Tool for Monitoring Key Elements of the Global Water Cycle, P Ieee, 98, 666-687, Doi 10.1109/Jproc.2010.2043032, 2010.

Kollet, S. J., Maxwell, R. M., Woodward, C. S., Smith, S., Vanderborght, J., Vereecken, H., and Simmer, C.: Proof of concept of regional scale hydrologic simulations at hydrologic resolution utilizing massively parallel computer resources, Water Resources Research, 46, 2010.

Lawrence, P. J., and Chase, T. N.: Representing a new MODIS consistent land surface in the Community Land Model (CLM 3.0), Journal of Geophysical Research: Biogeosciences, 112, 2007.

Lemaitre, F., Poussiere, J. C., Kerr, Y. H., Dejus, M., Durbe, R., de Rosnay, P., and Calvet, J. C.: Design and test of the ground-based L-band radiometer for estimating water in soils (LEWIS), Ieee Transactions on Geoscience and Remote Sensing, 42, 1666-1676, 10.1109/tgrs.2004.831230, 2004.

Lv, S., Zeng, Y., Wen, J., and Su, Z.: A reappraisal of global soil effective temperature schemes, Remote Sensing of Environment, 183, 144-153, 10.1016/j.rse.2016.05.012, 2016a.

Lv, S., Zeng, Y., Wen, J., Zheng, D., and Su, Z.: Determination of the Optimal Mounting Depth for Calculating Effective Soil Temperature at L-Band: Maqu Case, Remote Sensing, 8, 476, 2016b.

Lv, S., Zeng, Y., Wen, J., Zhao, H., and Su, Z.: Estimation of Penetration Depth from Soil Effective Temperature in Microwave Radiometry, Remote Sensing, 10, 519, 2018.

Lv, S., Zeng, Y., Su, Z., and Wen, J.: A Closed-Form Expression of Soil Temperature Sensing Depth at L-Band, IEEE Transactions on Geoscience and Remote Sensing, 1-9, 10.1109/TGRS.2019.2893687, 2019.

Njoku, E. G., and Kong, J.-A.: Theory for passive microwave remote-sensing of near-surface soil-moisture, Journal of Geophysical Research, 82, 3108-3118, 1977.

465 O'Neill, P., Chan, S., Njoku, E., Jackson, T., and Bindlish, R.: Soil Moisture Active Passive (SMAP),
466 Algorithm Theoretical Basis Document Level 2 & 3 Soil Moisture (Passive) Data Products, Revision B,
467 2015.
468 Ochsner, T. E., Cosh, M. H., Cuenca, R. H., Dorigo, W. A., Draper, C. S., Hagimoto, Y., Kerr, Y. H., Larson, K.
469 M., Njoku, E. G., Small, E. E., and Zreda, M.: State of the Art in Large-Scale Soil Moisture Monitoring, Soil
470 Sci Soc Am J, 77, 1888-1919, 10.2136/sssaj2013.03.0093, 2013.
471 Oleson, K., Niu, G. Y., Yang, Z. L., Lawrence, D., Thornton, P., Lawrence, P., Stöckli, R., Dickinson, R.,
472 Bonan, G., and Levis, S.: Improvements to the Community Land Model and their impact on the
473 hydrological cycle, Journal of Geophysical Research: Biogeosciences, 113, 2008.
474 Qin, J., Yang, K., Lu, N., Chen, Y. Y., Zhao, L., and Han, M. L.: Spatial upscaling of in-situ soil moisture
475 measurements based on MODIS-derived apparent thermal inertia, Remote Sensing of Environment, 138,
476 1-9, 10.1016/j.rse.2013.07.003, 2013.
477 Rosnay, P. d., Drusch, M., and Sabater, J. ı. M. n.: Milestone 1 Tech Note - Part 1: SMOS Global Surface
478 Emission Model, 2009.
479 Shrestha, P., Sulis, M., Masbou, M., Kollet, S., and Simmer, C.: A Scale-Consistent Terrestrial Systems
480 Modeling Platform Based on COSMO, CLM, and ParFlow, Monthly Weather Review, 142, 3466-3483,
481 10.1175/mwr-d-14-00029.1, 2014.
482 Sulis, M., Langensiepen, M., Shrestha, P., Schickling, A., Simmer, C., and Kollet, S. J.: Evaluating the
483 influence of plant-specific physiological parameterizations on the partitioning of land surface energy
484 fluxes, Journal of Hydrometeorology, 16, 517-533, 2015.
485 Tian, Y., Dickinson, R., Zhou, L., Zeng, X., Dai, Y., Myneni, R., Knyazikhin, Y., Zhang, X., Friedl, M., and Yu,
486 H.: Comparison of seasonal and spatial variations of leaf area index and fraction of absorbed
487 photosynthetically active radiation from Moderate Resolution Imaging Spectroradiometer (MODIS) and
488 Common Land Model, Journal of Geophysical Research: Atmospheres, 109, 2004.
489 Ulaby, F. T., Moore, R. K., and Fung, A. K.: Microwave Remote Sensing Active and Passive-Volume III:
490 From Theory to Applications, Artech House, Inc, 1986.
491 Vereecken, H., Huisman, J. A., Bogena, H., Vanderborght, J., Vrugt, J. A., and Hopmans, J. W.: On the
492 value of soil moisture measurements in vadose zone hydrology: A review, Water Resources Research,
493 44, 10.1029/2008wr006829, 2008.
494 Zeng, X., Shaikh, M., Dai, Y., Dickinson, R. E., and Myneni, R.: Coupling of the common land model to the
495 NCAR community climate model, Journal of Climate, 15, 1832-1854, 2002.

496